



Modeling elastic and inelastic, critical- and post-buckling behavior of bracing members

S. Krishnan¹

Abstract

An efficient beam element, the modified elastofiber (MEF) element, has been developed to capture the overall features of the elastic and inelastic responses of slender columns and braces under axial cyclic loading without unduly heavy discretization. It consists of three fiber segments, two at the member ends and one at midspan, with two elastic segments sandwiched in between. The segments are demarcated by two exterior nodes and four interior nodes. The fiber segments are divided into 20 fibers in the cross section that run the length of the segment. The fibers exhibit nonlinear axial stress-strain behavior akin to that observed in a standard tension test of a rod in the laboratory, with a linear elastic portion, a yield plateau, and a strain-hardening portion consisting of a segment of an ellipse. All the control points on the stress-strain law are user defined. The elastic buckling of a member is tracked by updating both exterior and interior nodal coordinates at each iteration of a time step and checking force equilibrium in the updated configuration. Inelastic post-buckling response is captured by fiber yielding, fracturing, and/or rupturing in the nonlinear segments. The key features of the element include the ability to model each member using a single element, easy incorporation of geometric imperfection, partial fixity support conditions, member susceptibility to fracture defined in a probabilistic manner, and fiber rupture leading to complete severing of the member. The element is calibrated to accurately predict the Euler critical buckling load of box and I sections with a wide range of slenderness ratios ($L/r=40, 80, 120, 160, \text{ and } 200$) and support conditions (pinned-pinned, pinned-fixed, and fixed-fixed). Elastic postbuckling of the Koiter-Roorda L frame (tubes and I sections) with various member slenderness ratios ($L/r=40, 80, 120, 160, \text{ and } 200$) is simulated and shown to compare well against second-order analytical approximations to the solution even when using a single-MEF element to model each leg of the frame. The inelastic behavior of struts under cyclic loading observed in the experiments of Black et al., Fell et al., and Tremblay et al. is accurately captured by single-MEF-element models. A FRAME3D model (using MEF elements for braces) of a full-scale six-story braced frame structure that was pseudodynamically tested at the Building Research Institute of Japan subjected to the 1978 Miyagi-Ken-Okai earthquake record is analyzed and shown to closely mimic the experimentally observed behavior.

¹ Assistant Professor of Structural Engineering and Geophysics, California Institute of Technology, krishnan@caltech.edu

1. Introduction

A cyclically, axially loaded slender element has a tendency to buckle laterally under compression, and straighten out and possibly yield in the ensuing tensile excursion. Subsequent loading cycles may result in localization of the buckled region at the mid-length of the member followed possibly by cracking and/or rupturing, ultimately severing the element completely. The buckling instability is greatly sensitive to end-fixity conditions and initial geometric imperfection. While the initial buckling may be a purely elastic phenomenon, subsequent compression excursions may result in significant inelastic buckling accompanied with a gradual or rapid degradation of the buckling strength. Thus, what starts out as a purely geometric nonlinearity evolves into a complex interplay between material and geometric nonlinearities, with the ductility of the material playing an important role in determining the low-cycle fatigue degradation and ultimate failure of the member. Accurately modeling such a multi-faceted phenomenon using a single element to represent the entire member is highly challenging, given the uncertainties associated with the member geometry including boundary conditions and the sensitivity of buckling response to the geometry. In addition, the ill-conditioning of the element stiffness matrix close to buckling and/or the stiffening of an imperfect or a buckled member due to a tensile excursion might make the solution difficult to converge numerically when using the tangent stiffness matrix for Newton-Raphson iterations. The objective of this study is to develop a beam-column element that can overcome these challenges and incorporate it into a previously developed 3-D analysis framework, FRAME3D (Krishnan 2003; Krishnan and Hall 2006a; Krishnan and Hall 2006b; Krishnan 2009a). The end goal is to be able to perform efficient and accurate 3-D collapse analysis of tall braced steel structures under strong earthquake ground motion.

2. The Modified Elastofiber (MEF) Element

Fiber elements have been successfully implemented to more accurately account for nonlinear material behavior under combined bending and axial load, including PMM interaction, strain hardening, cracking, and spread of nonlinearity along the member. Each element is divided into a number of segments and each segment is discretized into a number of fibers in the cross-section, with each fiber running the full length of the segment. Fully discretized fiber elements are computationally expensive, especially when implemented in a three-dimensional framework. Fortunately, in a series of cyclic load analyses conducted on isolated braces modeled using fully discretized 2-D Hall-Challa fiber elements (Hall and Challa 1995), Gan and Hall (1998) observed that strain is concentrated in a short segment at mid-span of braces with pinned ends, and in short segments at the two ends as well as at mid-span of braces with clamped ends. This observation suggests the possibility of efficiently, yet accurately, modeling braces by concentrating nonlinearity in short segments at the ends and at mid-span of the element. The modified elastofiber (MEF) beam element is designed to take advantage of this observed behavior. It is conceived as consisting of five segments delineated by six nodes (Fig. 1). The two exterior nodes, 1 and 2, coincide with one of the six attachment points or one of the eight panel corners of the adjacent panel zone elements at the left and the right. The four interior nodes, 3-6, separate the two end fiber segments and the central fiber segment from the two elastic segments. Each elastic segment is thus sandwiched between an end fiber segment and the central fiber segment. The elastic segments are elastic versions of the plastic hinge element (Krishnan and Hall 2006a), i.e., no

axial yielding and no plastic hinging. The fiber segment is based on the finite element method, wherein the beam translations and rotations are interpolated linearly and independently from their nodal values, requiring a one-point integration on the shear terms to prevent locking. Each fiber segment is discretized into 20 fibers that run the entire length of the segment. The arrangement of these fibers for wide-flange and box sections is shown in the figure. A fiber area zeroing capability is provided to adapt these layouts for angle, double-angle, channel, and T-sections.

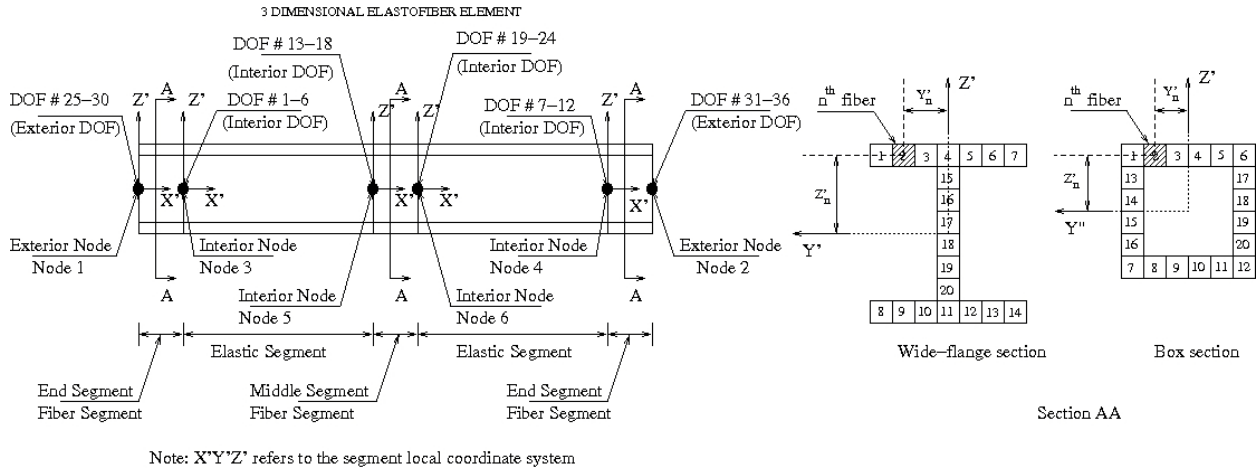


Figure 1. Layout of the five-segment modified elastofiber element.

Associated with each fiber is a nonlinear hysteretic stress-strain law, proposed by Hall and Challa (1995), for axial stress, σ_n , and axial strain, ϵ_n , where n denotes the n^{th} fiber. This hysteresis model defines a backbone curve (Fig. 2) consisting of a linear portion, a yield plateau, a strain-hardening region which is described by a cubic ellipse, and a strain softening region described by a continuation of the same cubic ellipse culminating in fiber rupture. The backbone curve is characterized by seven parameters: yield stress σ_y , ultimate stress σ_u , Young's modulus E , strain at initiation of strain hardening ϵ_{sh} , strain at ultimate stress ϵ_u , rupture strain ϵ_r , and the tangent modulus at initiation of strain hardening E_{sh} . Hysteresis loops consist of linear segments and cubic ellipses, and the hysteretic rules to define the cyclic response of each panel are given by (Challa 1992).

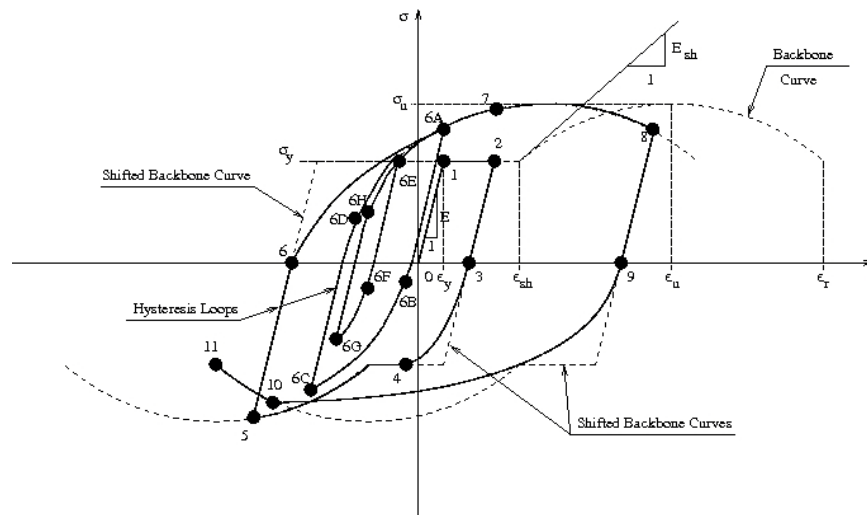


Figure 2. Axial stress-strain hysteresis model for each fiber.

Local buckling and fracture have been observed and reported in many cyclic axial load tests on braces (e.g., Tremblay et al. 2003, Han et al. 2007, and Fell et al. 2009). While the MEF element formulation is not amenable to the inclusion of local buckling, a fiber fracture capability, in the form of a user-specified probabilistic description of the fracture strain, is included to approximately represent brace fracturing. At the beginning of the analysis, the fracture strains for the fibers in all the MEF elements of the model are determined as independent realizations using the corresponding user-defined probability distributions. These initial fracture strains are held constant for the entire duration of the dynamic analysis. This method was first proposed by Hall (1998) to simulate fracture of welded beam-to-column connections in moment frames, accounting for variability and uncertainty in fracture initiation strains. It should be noted that this strain is an average fiber strain over the length of the entire segment, and does not correspond to the true strain in the continuum that can get much larger locally. When the fiber strain reaches the fracture strain, it fractures and can no longer take tension, but upon reversal of loading the fractured and separated parts can come in contact, and the fiber is able to resist compression again. This is, by design, unlike fiber rupture upon which the fiber can take no compression. Successive fracturing or rupturing of fibers can ultimately lead to complete severing of the brace. The phenomenological models of past studies incorporated fracture either by specifying the plastic rotation at fracture as a function of brace slenderness and plate width-to-thickness ratios (Tremblay et al. 2003) or by transforming the axial deformation history of the brace into standard cycles and assuming that the brace is fractured when the number of standard cycles exceeds a value that is dependent on the slenderness ratio, width-to-thickness ratio of the compression flange, width-to-depth ratio of the section, and the mechanical properties of steel (Tang and Goel 1989; Hassan and Goel 1991). Both methods postulate the instantaneous fracture of the entire cross-section. The MEF element overcomes this limitation by allowing fracture in one fiber to occur independently from another fiber, based solely on its instantaneous strain (although, since fiber strains must be consistent with nodal rotations, adjacent fibers tend to fracture at close time intervals especially under uniaxial bending conditions). Thus, fibers far away from the neutral axis, such as the flange fibers will fracture earlier than the web fibers, enabling partial and progressive fracture of the cross-section as observed in experiments. Assumptions in the MEF element formulation include prismatic sections, plane sections remain plane, small strains, no warping restraint, and no along-span loads. Lateral deflections relative to the chord in the two elastic segments are assumed small. Each of the six nodes of the MEF element have 6 degrees of freedom, three translational and three rotational. The interior nodes are assumed massless, and this allows for static condensation to be performed on the associated DOF, labeled 1–24 in Fig. 2. As a result, for each MEF element, updating the element stiffness matrix and the internal force vector requires an iterative nonlinear local structural analysis within each global iteration (Krishnan 2009b, 2010). The coordinates of the four interior nodes are updated at the end of each iteration. This geometric updating is critical for simulating large-deformation processes such as buckling. Using the updated configuration, the segment stiffness matrix and stiffness force vector are computed for each of the five segments as described in Krishnan and Hall (2006b), and assembled into the corresponding elemental quantities. For the three fiber segments, the incremental fiber strains are calculated from the incremental segment node displacements and rotations. If the beam ends are pinned ended, the contribution from the rotations is not included. For partially continuous connections, this contribution is scaled by two user-specified fixity factors (one for each end) ranging from zero to one, with zero corresponding to a perfectly pinned condition and one corresponding to full continuity. Using the fiber material model, and its axial

stress-strain history, the fiber axial stress is updated, and the new axial forces and bending moments at mid-length of the segments are computed. Shear forces, which are assumed constant along the beam at their values at segment mid-length to prevent shear locking, and twisting moments are also updated at this time. Using the values of internal forces at mid-length, the segment nodal forces are computed and assembled into the segment stiffness force vector. The two elastic segment stiffness matrices and force vectors are found by the procedure used for a plastic hinge element (Krishnan and Hall 2006a), except that no plastic hinges are allowed to form.

3. Handling of Specific Aspects of Compression Member Modeling

There are four key parameters of compression members that may have a significant role to play in the evolution of their critical and post-buckling behavior and the 5-segment layout of the MEF element lends itself to incorporate these parameters conveniently in a rational manner.

- (i) Initial Geometric Imperfection: The interior nodes of the middle fiber segment of the MEF element are initially displaced laterally based upon a user-specified major and/or minor direction eccentricity. This initial geometric imperfection can be input as a percentage of the length of the member. During the member iterations, the coordinates of the interior nodes are constantly updated starting from this imperfect initial configuration.
- (ii) Residual Stresses: Differential cooling results in non-uniform residual stresses in steel sections. Residual stresses can be easily incorporated into the MEF element by shifting the fiber stress-strain curve along the strain axis until the residual stress level is located at zero strain. Various levels of residual stresses can be assigned to various fibers of a fiber segment. However, this feature has not been included in the current version of FRAME3D.
- (iii) Loading history: In a series of cyclic axial loading experiments on 24 structural steel struts, Black et al. (1980) observed significantly different buckling loads for two identical specimen, one initially loaded and caused to yield in tension, and the other initially loaded in compression. They attributed this behavior to the Bauschinger effect that caused the stress-strain diagram in compression to be significantly rounded, reducing the elastic range of response. The MEF element will be able to approximately capture this effect since the hysteresis loops (Fig. 2) of the fiber axial stress-strain behavior consist of linear segments upon unloading to zero stress and cubic ellipses for further continuation of loading in the reverse direction.
- (iv) Gusset Plate Yielding: In cyclic loading tests on braces connected to supports through gusset plates, it has been observed that the gusset plates yield due to out-of-plane bending after just a few cycles. This causes the brace support condition to transition from a fixed end condition to a pinned end condition. The bending of gusset plates can be approximately modeled by matching the moment capacity of the gusset with a portion of the flange fibers of the end segments of the MEF element and zeroing the areas of the remaining fibers in the flanges. Another alternative is to use end-fixity factors smaller than unity.

4. Calibration

The generalized criterion for the selection of the fiber segment length in MEF elements is derived solely from its ability to predict the elastic critical buckling load for various cross-

sections, slenderness ratios, and support conditions. The Euler elastic critical buckling load for pinned ended members, fixed ended members, and members with one end pinned and one end fixed is π^2EI/L^2 , $4\pi^2EI/L^2$, and $2.0466\pi^2EI/L^2$, respectively. A single MEF element is used to model idealized struts with varying geometry, axially loaded in monotonically increasing compression. The struts are made of box (B8x8x3/16, B10x10x5/16, B12x12x7/16, and B14x14x1/2) and wide-flange (W8x20, W10x39, W12x72, and W14x90) sections, with varying slenderness ratios ($L/r = 40, 80, 120, 160$ and 200), and support conditions (pinned-pinned, pinned-fixed, and fixed-fixed). All the members are specified with large yield stresses such that they remain elastic until buckling. A fiber segment length of 2% of the element length gives the best predictions for the elastic critical buckling load, with over-prediction in roughly half the cases and under-prediction in the remaining cases. Prediction errors are under 3% in most cases with errors up to -11.5% in cases with the low KL/r of 20.

5. Validation

5.1 Elastic Post-Buckling Behavior of the Koiter-Roorda L-Frame

The L-shaped frame shown in Fig. 3 is loaded by a vertical force P at a small horizontal eccentricity “ e ” relative to the corner. The bars of the frame are of equal length and have equal uniform bending rigidities EI . Two buckling modes exist for the frame as shown in the figure. Simple free-body diagrams of the joint suggest three clear reasons for the inward buckling mode (shown in (c)) to be favored: (i) larger column axial force in this mode; (ii) beam is in compression in this mode reducing the flexural stiffness; (iii) curvature of the beam is smaller in this mode selectively facilitating this mode over the outward buckling mode. Numerical solutions using multiple elements to represent each bar, as well as semi-analytical solutions have been investigated in the past. Here, this frame is modeled using a single MEF element for each of the two bars. Multiple cases have been studied (box sections, B8x8x3/16 and B12x12x7/16; wide-flange sections, W10x39 and W14x90; bar slenderness ratios $L/r=40, 80, 120, 160$ and 200 ; applied load eccentricity $e=0.001L, 0.01L$ and $0.05L$). Shown in Fig. 3(d) is the comparison of the numerical solution against the approximate analytical second-order solution proposed by Bazant and Cedolin (1989) for the corner elastic rotation as a function of the axial force normalized by the critical buckling load of the perfect frame ($P_{CR} = 1.407\pi^2EI/L^2$), for one of the cases (W10x49, $L/R=200$). The single-MEF-element solution does quite well for reasonably large corner rotations. The smaller the applied loading eccentricity, the better the MEF element solution. The in-plane horizontal displacement of the corner is shown plotted in Fig. 3(e) to provide some insight into the extent of frame deformation until which the numerical solution is accurate. The results are excellent for corner displacements up to about 15% L , and they are satisfactory up to corner displacements of about 40% L . Modeling results for all the remaining cases are equally satisfactory (Krishnan 2009b, 2010).

5.2 Inelastic Buckling of Cyclically Loaded Struts in Pseudodynamic Tests

A series of cyclic load tests were conducted recently by Fell et al. on 19 tube (HSS, A500 Grade B), pipe (A53, Grade B), and wide-flange (A992) sections under the auspices of the Network for Earthquake Engineering Simulation (NEES) program, with the objective of investigating earthquake-induced buckling and fracture behavior (Fell et al. 2009). Three loading protocols

were used, a far-field loading protocol, and two near-fault – compression dominated and tension dominated – loading protocols that reflect demands imposed by near-fault ground motions. Another distinguishing feature of these tests was the use of typical braced frame connections, with the strut welded to a gusset plate that is bolted to the movable constraint frame and the stationary reaction block. The gusset plates were designed to preclude buckling. In fact, they yielded in out-of-plane plate bending in all the tests. While this resulted in an effectively pinned-end condition for the tube specimen (due to their superior out-of-plane stiffness dwarfing the low out-of-plane stiffness of the yielded gusset), partially fixed end conditions were created for the wide-flanged sections (whose lower out-of-plane stiffness is not enough to render the stiffness of the yielded gusset insignificant). The investigators paid close attention to the onset of local buckling and fracture and catalogued these events for each test. In this study, the Fell et al. specimen utilizing HSS and wide-flange sections are modeled using single MEF elements.

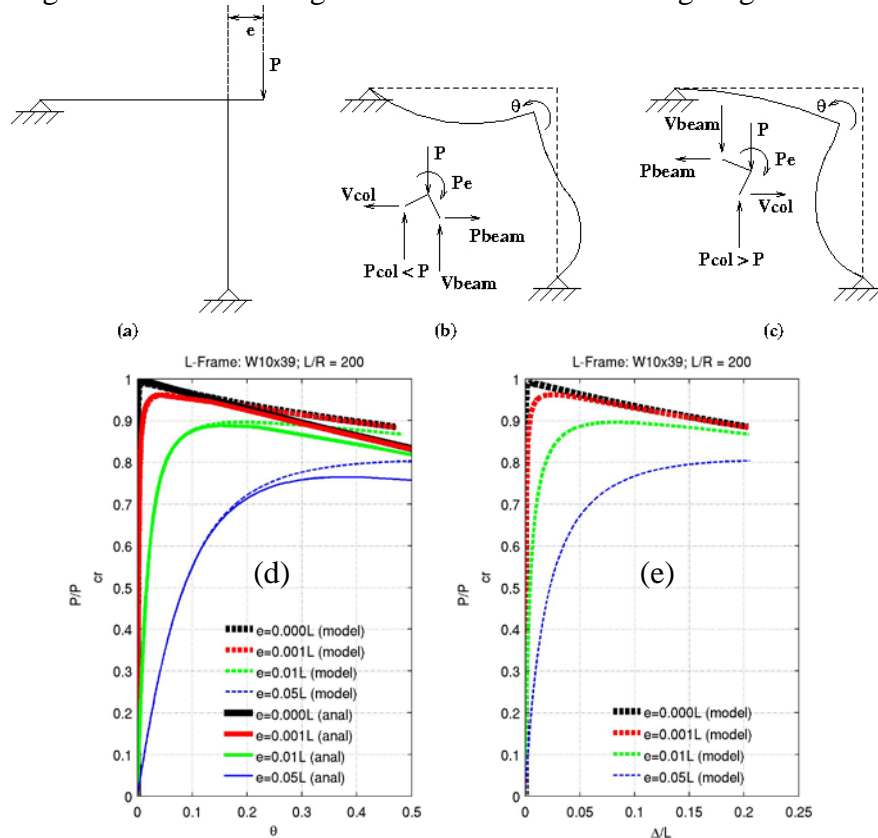


Figure 3. (a) Undeformed geometry of the L-shaped Koiter-Roorda frame eccentrically loaded at the corner. (b) and (c) Two possible buckling modes (after Bazant and Cedolin). The force equilibrium at the joint is shown for both cases. Buckling to the left (c) is favored. (d) Comparison of the numerical solution for the corner rotation using MEF elements against a second-order analytical solution for a W10x39, $L/R=200$ frame. (e) Corner in-plane lateral displacement versus P/P_{CR} .

Specimen #2 (HSS 4x4x1/4) was subjected to an asymmetric compression-dominated near-field loading history. In the first strong cycle, the brace was loaded to 2% drift angle in tension, followed by 6% drift angle in compression. The brace yielded and elongated in the first tensile excursion, significantly lowering the compressive buckling load. Local buckling was observed during the first large compression excursion (at a drift of 2.5%). The brace cycled at a residual drift of 3% for the remainder of the test. The MEF element is able to capture the hysteretic

behavior accurately as evidenced by the agreement in the observed and computed axial force – axial deformation and axial force – lateral deformation histories shown in Fig. 4. The tensile severing of the brace is not adequately captured, however the lateral deformation of the brace agrees quite well with the experiment.

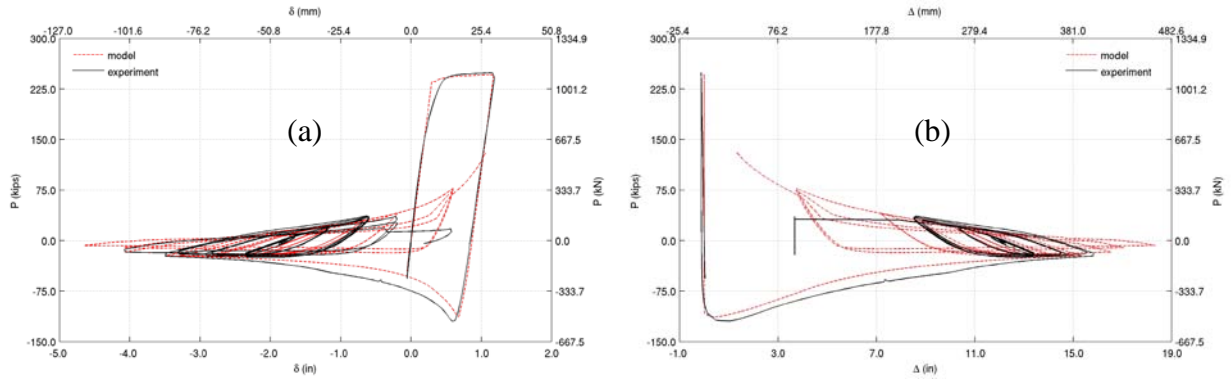


Figure 4. Comparison of simulation against data from Fell et al. test 2 on HSS4x4x1/4 ($KL/r \approx 80$): (a) Axial displacement versus axial force history; (b) Minor direction lateral displacement versus axial force history.

5.3 Analytical Simulation of the Full-Scale Pseudodynamic Test of a 6-Story Steel Building

In the years 1982–1984, a full-scale six-story braced steel building was designed, constructed, and tested at the Building Research Institute (BRI) in Tsukuba, Japan, under a US-Japan cooperative research program (Foutch et al. 1987; Roeder et al. 1987; Midorikawa et al. 1989). Three pseudodynamic tests were conducted using the N-S component of the Tohoku University accelerogram recorded during the July 12, 1978, Miyagi-Ken-Oki earthquake, which had a peak acceleration of 2.58m/s^2 : an “elastic” test with a peak acceleration of 0.65m/s^2 , a “moderate” test with a peak acceleration of 2.50m/s^2 , and an “inelastic final” test with a peak acceleration of 5.00m/s^2 . The simulated response (Figs. 5 and 6) from a tuned FRAME3D model with each brace modeled by a single MEF element compares remarkably well against data from the experiment. Greater details can be found in Krishnan (2009b, 2010).

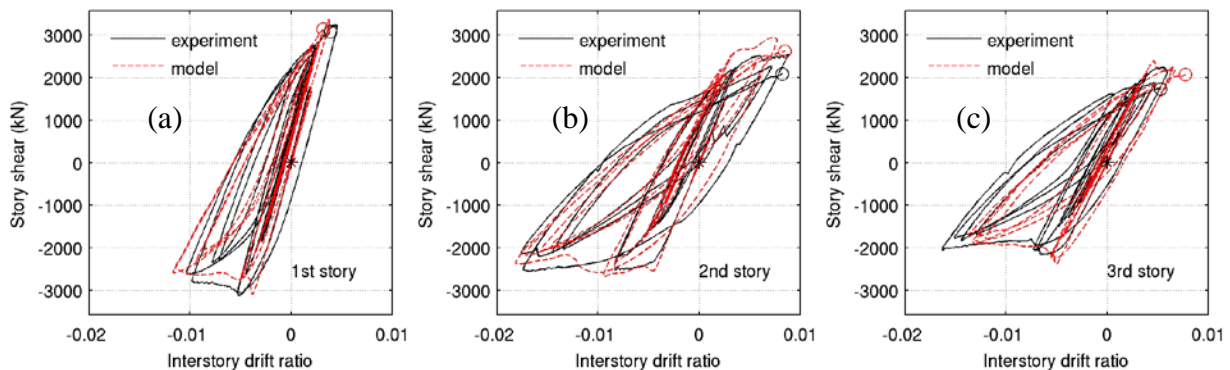


Figure 5. Comparison of analytical and experimental inter-story drift ratio versus story shear of the 6-story test structure (1st, 2nd, and 3rd stories).

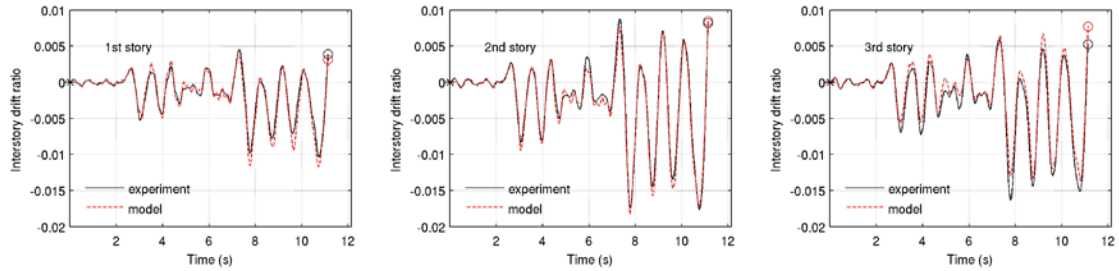


Figure 6. Comparison of analytical and experimental inter-story drift ratio response histories of the 6-story test structure (1st, 2nd, and 3rd stories).

6. Conclusions

A beam-column element termed the modified elastofiber (MEF) element has been developed to efficiently model buckling-sensitive slender columns and braces in steel structures. The element consists of 5 segments, 3 nonlinear fiber segments - two at the ends and one at mid-span, and 2 elastic segments sandwiched between the nonlinear segments. It is designed to simulate yielding at the element ends and first mode buckling. A local geometry-updating feature is used to track interior node displacements as the element buckles. A unique feature of the element is the capability to model fracture and rupture of fibers in the plastic-hinging region of the brace, leading to its complete severing. The ability of the element to simulate elastic post-buckling behavior and inelastic buckling under cyclic loading has been validated using analytical solutions (Koiter-Roorda L-frame) and experimental data (Black et al., Fell et al., and Tremblay et al. tests). An assembled FRAME3D model of a 6-story test structure using MEF elements for braces is able to capture experimentally measured response under pseudodynamically implemented earthquake shaking quite well.

Acknowledgments

The author is grateful to Prof. Chia-Ming Uang (University of California, San Diego) for providing data from the US-Japan pseudodynamic test of the 6-story structure, to Prof. Robert Tremblay (Ecole Polytechnique, Montreal, Canada) for providing data from his tests on concentrically braced steel frames, to Prof. Amit Kanvinde (University of California, Davis) and Prof. Benjamin Fell (California State University, Sacramento), for extensive discussions on brace behavior and for providing the data from their NEESR brace-testing project.

References

- Bazant, Z. P. and Cedolin, L. (1989). "Initial post-critical analysis of asymmetric bifurcation in frames". *Journal of Structural Engineering*, 115 (11) 2845-2857.
- Black, G.R., Wenger, W.A., and Popov, E.P. (1980). "Inelastic buckling of steel struts under cyclic load Reversals". Tech. Rep. UCB/EERC-80-40, University of California, Berkeley, California.
- Challa, V.R.M. (1992). "Nonlinear seismic behavior of steel planar moment-resisting frames". Tech. Rep. EERL 92-01, Caltech, Pasadena, California.
- Fell, B.V., Kanvinde, A.M., Deierlein, G.G., and Myers, A.T. (2009). "Experimental investigation of inelastic cyclic buckling and fracture of steel braces". *Journal of Structural Engineering* 135 (1) 19-22.

- Foutch, D.A., Goel, S.C., and Roeder, C.W. (1987). "Seismic testing of full-scale steel building - Part I." *Journal of Structural Engineering* 113 (11) 2111–2129.
- Gan, W. and Hall, J.F. (1998). "Static and dynamic behavior of steel braces under cyclic displacement". *Journal of Engineering Mechanics* 124 (1) 87-93.
- Hall, J.F. (1998). "Seismic response of steel frame buildings to near-source ground motions". *Earthquake Engineering and Structural Dynamics* 27 (12) 1445–1464.
- Hall, J.F. and Challa, V.R.M. (1995). "Beam-column modeling". *Journal of Engineering Mechanics* 121 (12) 1284-1291.
- Han, S.-W., Kim, W.T., and Foutch, D.A. (2007). "Seismic behavior of HSS bracing members according to width-thickness ratio under symmetric cyclic loading". *Journal of Structural Engineering* 133 (2) 264-273.
- Hassan, O.F. and Goel, S.C. (1991). "Modeling of bracing members and seismic behavior of concentrically braced steel structures". Tech. Rep. UMCE 91-1, Univ. of Michigan, Ann Arbor, Michigan.
- Krishnan, S. (2003). "FRAME3D - A program for three-dimensional nonlinear time-history analysis of steel buildings: User guide". Tech. Rep. EERL 2003-03, Caltech, Pasadena, California.
- Krishnan, S. (2009a). "FRAME3D V2.0 - A Program for the Three-Dimensional Nonlinear Time-History Analysis of Steel Buildings: User Guide". Tech. Rep. EERL 2009-04, Caltech, Pasadena, California.
- Krishnan, S. (2009b). "On the modeling of elastic and inelastic, critical- and post-buckling behavior of slender columns and bracing members". Tech. Rep. EERL 2009-03, Caltech, Pasadena.
- Krishnan, S. (2010). "Modified elastofiber element for steel slender column and brace modeling". *Journal of Structural Engineering* 136 (11) 1350-1366.
- Krishnan, S. and Hall, J.F. (2006a). "Modeling steel frame buildings in three dimensions - Part I: Panel zone and plastic hinge beam elements". *Journal of Engineering Mechanics* 132 (4) 345-358.
- Krishnan, S. and Hall, J.F. (2006b). "Modeling steel frame buildings in three dimensions - Part II: Elastofiber beam element and examples". *Journal of Engineering Mechanics* 132 (4) 359-374.